

## REYNOLDS NUMBER EFFECTS ON STATISTICS AND STRUCTURE OF AN ISOTHERMAL REACTING TURBULENT WALL-JET

Zeinab Pouransari and Arne V. Johansson

Linné FLOW Centre, Dept. of Mechanics,  
Royal Institute of Technology  
SE-100 44 Stockholm, Sweden  
zeinab@mech.kth.se

### ABSTRACT

In this study, three-dimensional direct numerical simulation (DNS) is used to investigate a reacting turbulent wall-jet. The flow is compressible and a single-step global reaction is considered. At the inlet, fuel and oxidizer enter the domain separately in a non-premixed manner. Two different simulations with different Reynolds numbers,  $Re = 2000$  and  $Re = 6000$  in terms of the inlet quantities are considered. The DNS-database of Pouransari *et al.* (2011) with the lower Reynolds number is used here for comparison and a new DNS is performed, in which the bulk Reynolds number is increased by a factor of three. This results in a comparable increase in the friction Reynolds number, which allows the study of Reynolds number effects. The main objective of this study is to compare the influences of changing the Reynolds number of the flow with the heat-release effects caused by the chemical reaction, that we studied earlier in Pouransari *et al.* (2013). Results primarily show that, the Reynolds number effects can clearly be observed both in turbulent structures and in the flame characteristics. While, both turbulent and flame structures become finer at the higher Reynolds number, the effect of decreasing the Reynolds number and adding the combustion heat release are not always the same.

### INTRODUCTION

Many different numerical studies have been performed on various aspects of turbulent combustion in several flow configurations. However, in most of these studies, in particular when direct numerical simulation is employed as the computational tool, the Reynolds number of the flow is very limited and much lower than in real physical situations. Thus, some of the conclusions drawn in these cases, may be subject to both qualitative and quantitative changes at higher Reynolds numbers.

Effects of Reynolds number in most canonical flows have been addressed both numerically and experimentally. Such as in turbulent channel flow (Hoyas & Jiménez, 2008; Wei & Willmarth, 1989), turbulent boundary layers, (DeGraaff *et al.*, 1998), and pipe flows (Den Toonder & Nieuwstadt, 1997). Some studies on the scaling properties have also been performed to capture these dependencies. Today, the Reynolds number of experimental facilities has increased substantially and both smooth and rough wall flows are still of great interest, see Hong *et al.* (2011); Bailey *et al.* (2013). It is only in the last

few years that DNS studies have reached Reynolds numbers where significant scale separation (between inner and outer scales) can be claimed.

Many other efforts in the study of the Reynolds number effects are directed towards the degree of local isotropy and the fine structures of turbulence. For these purposes, experiments and numerical investigations with different Reynolds numbers are considered and in general at higher Reynolds numbers a high degree of universality of small scales and local isotropy have been found, see Ferchichi & Tavoularis (2000); Yiu *et al.* (2004); Schumacher (2008).

Reynolds number effects on scalar dissipation rate transport and its modeling in turbulent premixed combustion is addressed by Chakraborty & Swaminathan (2013). They have used scaling arguments to explain the effects of Reynolds number on the turbulent transport, scalar-turbulence interaction and the combined reaction and molecular dissipation terms. They found that the modeling of the term arising from density variation has no significant Reynolds number dependence (within the range examined).

DNS is a reliable tool for the study of various turbulent flows. However, some cases such as compressible and reacting flows are computationally more demanding and hence numerical studies of turbulent combustion flows are usually restricted to lower Reynolds number ranges, (Peters, 2000; Vervisch & Poinso, 1998).

In our previous studies of wall-jet flows, we have addressed the turbulent flow effects on the structure of the flame both in the absence and presence of combustion heat-release, (Pouransari *et al.*, 2011, 2013). However, in those studies, we kept the bulk Reynolds number constant and focused on the heat-release and turbulence interactions. In the present study, the bulk Reynolds number is increased by a factor of three, which results in a comparable increase in the friction Reynolds number. In the present investigation, the Reynolds number effects in a reacting turbulent wall-jet are considered. In particular, we are interested in comparing these effects which we observed in the study of the heat-release effects at the higher Reynolds number where the scale separation starts to become significant. In general, including the combustion heat-release in a reacting turbulent flow decreases the local Reynolds number. Thus, in our previous studies on the effects of heat-release in a reacting turbulent wall-jet; we observed different changes in the mixing scales of the flow. There, we examined how the presence of heat-release could affect the scales of turbulence and in return how it can affect the global reaction. Here, we dis-

regard the heat-release effects, and instead change the bulk Reynolds number of the flow. Therefore, we can study the Reynolds number effects on the isothermal reaction and on the structure and statistics of the flow, in the absence of thermal effects.

## Governing equations

The conservation equations of total mass, momentum and energy read

$$\frac{\partial \rho}{\partial t} + \frac{\partial \rho u_j}{\partial x_j} = 0 \quad (1)$$

$$\frac{\partial \rho u_i}{\partial t} + \frac{\partial \rho u_i u_j}{\partial x_j} = -\frac{\partial p}{\partial x_i} + \frac{\partial \tau_{ij}}{\partial x_j} \quad (2)$$

$$\frac{\partial \rho E}{\partial t} + \frac{\partial \rho E u_j}{\partial x_j} = -\frac{\partial q_i}{\partial x_i} + \frac{\partial (u_i (\tau_{ij} - p \delta_{ij}))}{\partial x_j}. \quad (3)$$

Here  $\rho$  is the total mass density,  $u_i$  are the velocity components,  $p$  is the pressure and  $E = e + \frac{1}{2} u_i u_i$  is the total energy. The summation convention over repeated indices is used. The heat fluxes are approximated by the Fourier's law according to  $q_i = -\lambda \frac{\partial T}{\partial x_i}$ , where  $\lambda$  is the coefficient of thermal conductivity and  $T$  is the temperature. The viscous stress tensor is defined as  $\tau_{ij} = \mu \left( \frac{\partial u_i}{\partial x_j} + \frac{\partial u_j}{\partial x_i} \right) - \mu \frac{2}{3} \frac{\partial u_k}{\partial x_k} \delta_{ij}$  where  $\mu$  is the dynamic viscosity. The fluid is assumed to be calorically perfect and to obey the ideal gas law according to  $e = c_v T$ ,  $p = \rho R T$ , and a ratio of specific heats of  $\gamma = c_p / c_v = 1.4$  is used. The viscosity is determined through the Sutherland's law  $\frac{\mu}{\mu_j} = \left( \frac{T}{T_j} \right)^{3/2} \frac{T_j + S_0}{T + S_0}$ , where  $T$  is the local temperature,  $T_j$  is the jet center temperature at the inlet and  $S_0$  is a reference value, taken as  $S_0 = 110.4 K$ .

Conservation of the species masses is governed by

$$\frac{\partial \rho \theta_k}{\partial t} + \frac{\partial}{\partial x_j} (\rho \theta_k u_j) = \frac{\partial}{\partial x_j} \left( \rho \mathcal{D} \frac{\partial \theta_k}{\partial x_j} \right) + \dot{\omega}_k, \quad (4)$$

where  $\theta_k$  and  $\dot{\omega}_k$  are the mass fractions and the reaction rate of the oxidizer, fuel and passive scalar species. An equal diffusion coefficient  $\mathcal{D}$  for all scalars, is used to approximate the diffusive fluxes.

The simulated reaction is modeled by a single-step irreversible reaction between oxidizer species  $O$  and fuel species  $F$  that react to form a product  $P$ , which is described as  $\nu_O O + \nu_F F \rightarrow \nu_P P$ . Stoichiometric coefficients of one are used for all species and the molecular weights are also assumed to be equal for the reactants. The reaction mass rate is formulated as  $\dot{\omega} = k_r \rho^2 \theta_O \theta_F$ . The reaction rate is prescribed by a Damköhler number of  $Da = \frac{\tau_{conv}}{\tau_{react}} = \frac{h}{U_j} k_r \rho_j = 3$ , where  $k_r$  is the reaction rate and  $U_j$  and  $\rho_j$  are the center-line velocity and the density of the jet at the inlet. No heat release is used in the present simulation and only the oxidizer and fuel mass fractions are computed since the product does not enter in the reaction rate expression. Since the flow is uncoupled from the reactions, the influence of increasing the Reynolds number can be studied in the absence of temperature effects. Apart from reacting species, a passive scalar equation is also solved for comparison.

## Numerical method and parameters

A fully compressible Navier-Stokes solver is employed for simulation of the wall-jet. The code uses a sixth-order

compact finite difference scheme for spatial discretization and a third-order Runge-Kutta method for the temporal integration.

Table 1. Parameters of direct numerical simulations of reacting turbulent wall jet flows;  $Pr = 0.7$ ,  $Sc = 0.7$  and  $Da = 3$  in both of the simulations

Case	$L_x \times L_y \times L_z$	$N_x \times N_y \times N_z$	$Re$
I	$35 \times 17 \times 7.2$	$320 \times 192 \times 128$	2000
II	$35 \times 14 \times 7.2$	$960 \times 480 \times 384$	6000

The computational domain is a rectangular box of size  $[L_x \times L_y \times L_z = 35h \times 17h \times 3.6h]$  where  $L_x$ ,  $L_y$  and  $L_z$  denote dimensions in the streamwise, wall-normal and spanwise directions, respectively, and  $h$  is the inlet jet height. The number of grid points are  $[N_x \times N_y \times N_z = 960 \times 480 \times 384]$  and the inlet based Reynolds number of the wall-jet is  $Re = 6000$ . In the remaining of this paper, this case is referred to as case II, while the DNS data in paper Pouransari *et al.* (2011) is tagged as case I, in which the grid points were  $[N_x \times N_y \times N_z = 320 \times 192 \times 128]$  and  $Re = 2000$ . The density and temperature are varied over the jet profile and the wall temperature is kept constant and equal to the ambient flow temperature. The specifications are summarized given in Table 1.

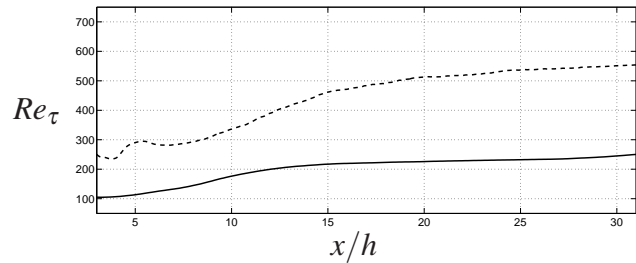


Figure 1. Downstream development of the friction Reynolds number; solid line: case I ( $Re = 2000$ ) and dashed line: case II ( $Re = 6000$ ).

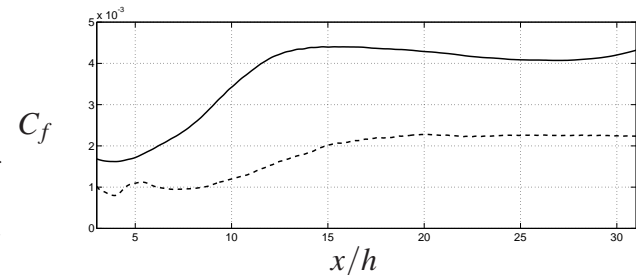


Figure 2. Downstream development of the skin friction coefficient.

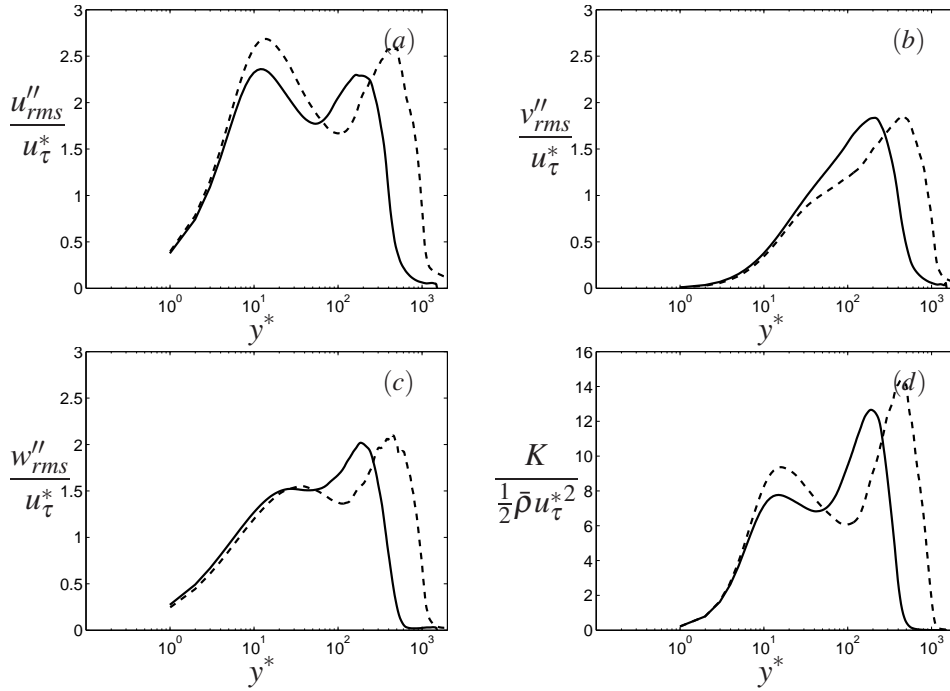


Figure 3. (a) Streamwise, (b) wall-normal, (c) spanwise fluctuation intensity and (d) Mean turbulent kinetic energy using semi-local normalization defined as  $u_\tau^* = \sqrt{\bar{\rho}_w/\bar{\rho}} u_\tau$  and  $l^* = \frac{(\bar{\mu}/\bar{\rho})}{u_\tau^*} = \frac{(\bar{\mu}/\bar{\rho})}{\bar{\rho}/\bar{\rho}_w} l^+$ , where  $u_\tau = \sqrt{\bar{\tau}_w/\bar{\rho}_w}$  and  $l^+ = \bar{v}_w/u_\tau$  are the friction velocity and length scales, and wall conditions are denoted by a subscript  $w$ . Profiles at  $x/h = 25$ .

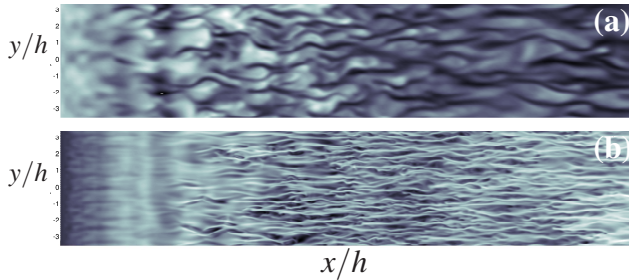


Figure 4. Instantaneous snapshots of the streamwise velocity fluctuations at  $y^+ \approx 8$  for (a) case I and (b) case II; Light and dark colors represent positive and negative fluctuations.

## RESULTS AND DISCUSSIONS

### Turbulent statistics and flow structure

To get a general insight into the two cases with different bulk Reynolds number we examine the friction Reynolds number  $Re_\tau = u_\tau \delta/v_w$ , see figure 1. In this figure a dashed line is used for case II and a solid line for case I. Note that these line styles are used throughout the paper unless otherwise stated. When an appropriate outer length-scale  $\delta$  is used, the friction Reynolds number can be seen as an estimate of the outer-layer to inner-layer length-scale ratio. Around  $x/h = 25$ , for case II ( $Re = 6000$ ) the friction Reynolds number reaches the value of  $Re_\tau = 540$  and for case I ( $Re = 2000$ ) it reaches  $Re_\tau = 220$ .

The accurate experimental determination of the skin friction still remains to be a major challenge in turbulent wall flows.

The values of the skin friction coefficients,  $C_f = 2(u_\tau/U_m)^2$  are shown in figure 2 for cases I and II. At the downstream position  $x/h = 15$ , for instance, in the transition region, the  $C_f$  coefficient is more than 55% lower for

case I compared to case II. In the fully turbulent region, at  $x/h = 25$ , it is about 50% lower. These observations can, in some sense, be seen in analogy with the reductions in  $C_f$  observed when heat release effects were added (to the low  $Re$  case) and hereby further reduced the Reynolds number, see Pouransari & Johansson (2011).

The averaged turbulence intensity for the three components of the velocity are plotted in figure 3(a-c) using semi-local inner scaling. The turbulent kinetic energy is plotted in figure 3(d) using the same normalization. With this scaling we observe a good collapse in the near-wall region, up to  $y^+ = 7 - 8$ . In order to make the comparison easier, the same scaling method is used later for plotting the two-dimensional spectra. For details of this normalization see Pouransari *et al.* (2013). Figure 3(a) shows that increasing the Reynolds number, will increase the fluctuation intensities in the streamwise direction both in the inner and outer regions. It is a clear increase in the amplitude of the two peaks of the fluctuation intensity and also as a assign of increase in the Reynolds number they get further separated from each other. For the spanwise component, figure 3(c), the peak of the fluctuation profile slightly increases with increasing of the Reynolds number and also gets further away from the wall. Figure 3(b) shows that the wall-normal velocity fluctuations in some regions decreases when the Reynolds number increases, this behavior is the same if the absolute values are considered without any scaling. The peak value seems to be unaffected for the two Reynolds numbers considered. What is consistent, using different scalings, is that due to increasing the Reynolds number, the outer maximum is shifted further outward from the wall region and the locations of the two peaks get further separated from each other for all components of the fluctuations. As a result, the same trend is observed in the turbulent kinetic energy profile (figure 3(d)). The advantage of using the semi-local scaling is the good collapse of

the profiles in the near-wall region for the two cases with different Reynolds numbers.

To identify and explain the influences of Reynolds number effects on the structure of the turbulent wall-jet and to have a general idea about the flow field, the streamwise velocity fluctuations are plotted. Visualizations of the instantaneous fields indicate that the jet is fully turbulent beyond  $x/h \approx 15$ . Figure 4(a) shows the instantaneous fluctuations of the streamwise velocity in the  $xz$ -plane at  $y^+ \approx 8$ . Elongated streamwise streaks, typically present in the viscous sublayer of wall flows are also seen in the turbulent wall-jets presented here. It is clearly observed that due to increasing the Reynolds number the distances between the streaks decreases and therefore the two point correlation profiles of velocities are modified.

The turbulent flow structure near the walls is significantly different at high Reynolds number compared to the lower Reynolds number. For instance, the hair-pin and vorticity structures and their interactions will be evolved and modified going from low Reynolds number to high Reynolds number cases. However, for the range of Reynolds numbers considered in this study, the general form of the structures remain fairly similar between the cases. The size of the streaks is changing with the Reynolds number. To determine the size of the turbulence structures in the near-wall region, two-point correlations,  $R_{u_i u_i}(x, y, r) = \overline{u_i''(x, y, z, t) u_i''(x, y, z + r, t)}$ , of the fluctuating velocities in the spanwise direction, at  $y^+ = 8$  are calculated and the corresponding one dimensional spectra in each direction are obtained.

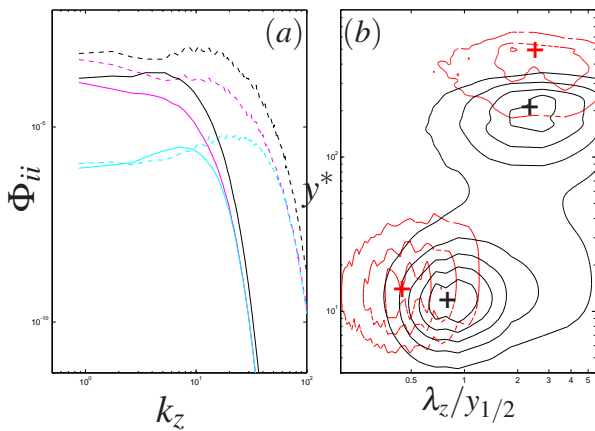


Figure 5. (a) One-dimensional spanwise spectra,  $\Phi_{ii}$ , at  $y^+ = 8$ . Color code as follows, streamwise:  $\Phi_{11}$  (black), wall-normal:  $\Phi_{22}$  (cyan) and spanwise:  $\Phi_{33}$  (magenta); (b) Premultiplied spanwise spectra,  $E_{uu}^z = \lambda_z \Phi_{uu} / u_{\tau}^{*2}$ , of the streamwise velocity fluctuations, case I (black, solid) and case II (red, dashed), scaled in the semi-local inner scaling; Contours at  $x/h = 25$ .

Reynolds number influences on turbulence scales in the near-wall region of the wall-jet flow can be illustrated by examining the one-dimensional spanwise spectra close to the wall. Figure 5(a) shows the one-dimensional spectra at  $y^+ = 8$  of the three velocity components as function of the spanwise wavenumber in outer units. As we should expect, one can observe an increase in the range of scales that is essentially proportional to the increase in Reynolds

number. The spectrum of the streamwise velocity is clearly influenced at all wave-numbers. The general increase in the turbulence energy of figure 3(d), is also clearly reflected in the spectra. However, increasing the Reynolds number has affected different components in an anisotropic manner. While the energy content at low wave numbers both for the streamwise and spanwise components is substantially increased, it is almost unaffected for the wall-normal component.

A more comprehensive insight can also be gained by examining the two-dimensional spectra, see del Álamo & Jiménez (2003). The two-dimensional premultiplied spectra,  $E_{uu}^z = \lambda_z \Phi_{uu} / u_{\tau}^{*2}$  of the streamwise velocity fluctuations as a function of spanwise wavenumber and wall-normal position are shown in figure 5(b), in inner units, for two cases. Here, we have used the semi-local inner scaling as,  $E_{uu}^{z*} = \lambda_z \Phi_{uu} / u_{\tau}^{*2}$ ; A corresponding wavelength, as  $\lambda_z^* = (2\pi / \kappa_z) u_{\tau}^* / \nu$ , could not be defined, due to the density variation along the wall-normal axis, see Pouransari *et al.* (2013). Here,  $\lambda_z = 2\pi / \kappa_z$  is the wavelength and is scaled with the corresponding local half-height of the jet for each case. The spectra have two peaks. The inner peak, which corresponds to the near-wall streaks, is located almost at the same wall-distance, in terms of semi-local inner scaling ( $y^*$ ) for the two cases. The outer-peak, which corresponds to the large energetic structures of the outer-layer, is located at different distances from the wall for the two cases, when inner scaling is used. This behavior is consistent with the observations made in the profiles of the turbulence kinetic energy. The peaks would essentially coincide for outer scaling ( $y/y_{1/2}$ ). The figure confirms that the inner peak location is shifted to smaller scales. Though,  $\lambda_z^*$  cannot be used for the whole figure. One can estimate the locations of the peak in terms of  $\lambda_z^*$  would be roughly the same for two cases. In outer scaling  $\lambda_z / y_{1/2}$ , the outer peak for the higher Reynolds number is only slightly shifted to higher values.

## Scalar statistics and flame structure

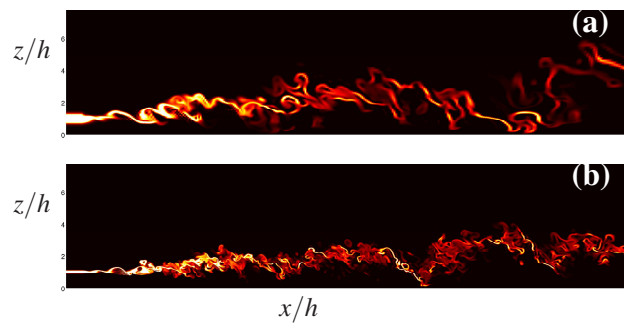


Figure 6. Instantaneous snapshots of the reaction rate fields for (a) case I and (b) case II; The lighter color indicates higher reaction rates.

The snapshots of the reaction term for both cases are presented in figure 6. These plots show that the reaction mainly occurs in the upper shear layer in thin sheet-like structures, but also takes place near the wall. Figure 6 confirms that the flame gets much more wrinkled as the Reynolds number increases. The structure of the flame is affected both in the outer layer, close to the half-height of

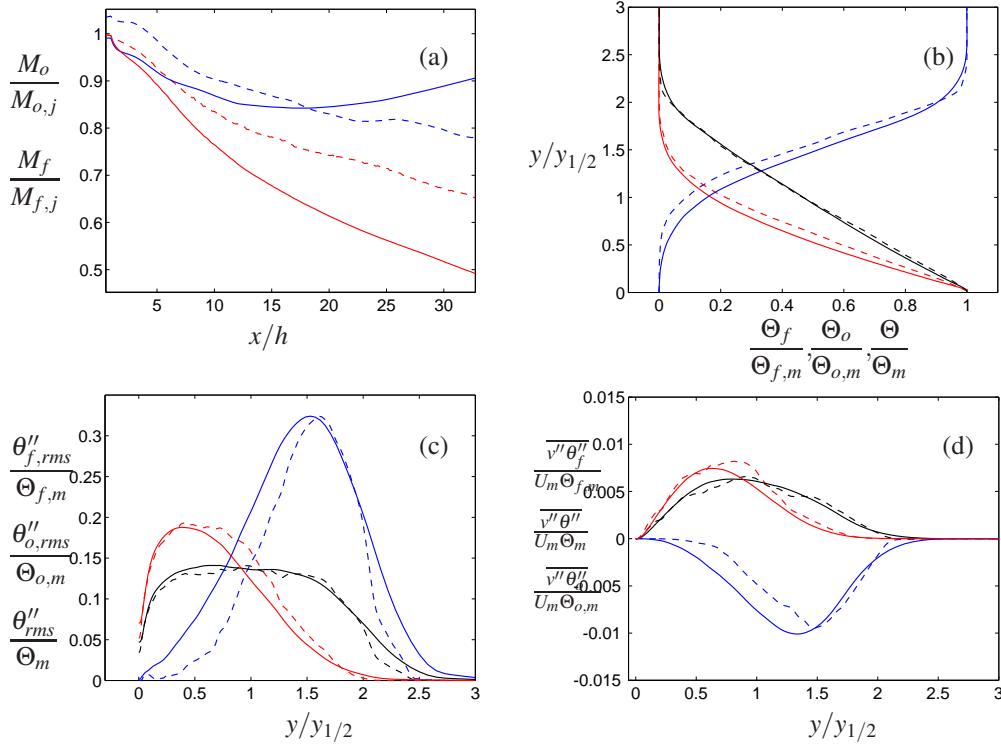


Figure 8. (a) Reactants mass flux and (b) cross-stream profiles of the mean values, (c) fluctuation intensity and (d) wall-normal fluxes of the scalars; oxidizer: blue, fuel: red, passive: black; Subscript  $m$  refers to the maximum value.

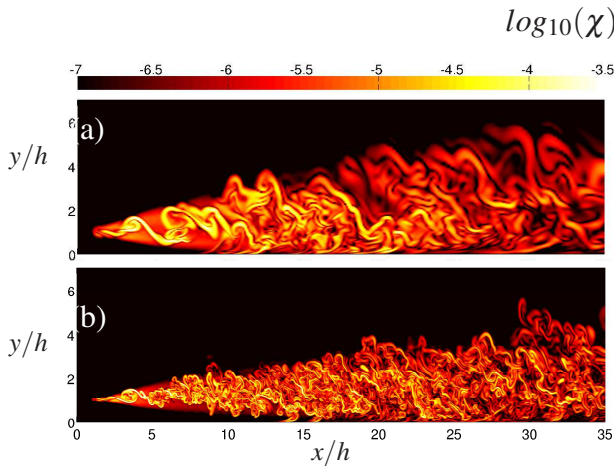


Figure 7. Iso-contours of the logarithm of the instantaneous scalar dissipation rate, (a) case I and (b) case II.

the jet, and in the near-wall region. However, even though that the flame gets much more wrinkled and folded in different regions, in general also gets somewhat thinner and becomes more intensified and concentrated.

The scalar dissipation rate is a quantity of prominent importance in non-premixed combustion. The Reynolds number effects on the scalar dissipation rate are illustrated in figure 7 where the iso-contours of the scalar dissipation rate for two cases are shown. The fields are plotted on a logarithmic scale to accentuate their wide dynamic range. The flow is fully turbulent in both cases and long thin sheet-like structures are observed, similar to what is reported by Hawkes *et al.* (2007). These figures show much finer scale structures in the dissipation rate field of case II, indicating generation of more small scales due to the increase in the

Reynolds number. In the study by Pouransari *et al.* (2013), we observed how the combustion heat release can damp the scales and perhaps merge them to larger structures, the higher Reynolds number effects is clearly the opposite and the structures are getting finer at the higher Reynolds number. In a non-reacting flow, one expect that the scalar dissipation rate fluctuations increase with the Reynolds number, however, here in the reacting turbulent wall-jet flow we need to examine the fluctuations of the scalars.

Different statistics of the reacting and passive scalars are shown in figure 8. The downstream development of the fuel and oxidizer mass fluxes are plotted in figure 8(a), which shows that the fuel species are consumed faster at the lower Reynolds number case, at  $x/h=30$  for example about 40 % less fuel is consumed in the higher Reynolds number case compared to case I. Thus, the rate of fuel consumption is decreased by increasing the Reynolds number. Moving further downstream, the oxidizer mass flux in both cases increase after  $x/h = 17$ , as a result of the oxidizer influx at the top of the domain. The cross-stream profiles of the scalar concentrations are displayed in figure 8(b). This plot confirms that for both non-reacting and reacting scalar, the profiles of different cases collapse when outer scaling is used. As seen in figure 8(c), the fluctuation level of the scalars has only weakly been affected by increasing the Reynolds number. The peaks of the profiles are almost unchanged. This is clearly contrary to the heat-release effects, where the influences were considerable, see Pouransari *et al.* (2013). The wall-normal fluxes, shown in figure 8(d), exhibit a similar behavior.

## REFERENCES

- Bailey, S., Hultmark, M., Monty, J., Alfredsson, P.H., Chong, M., Duncan, R., Fransson, J. H. M., Hutchins,



August 28 - 30, 2013 Poitiers, France

- N., Marusic, I., McKeon, B. J., Nagib, H.M., Örlü, R., Segalini, A. S., Smits, A. J. & Vinuesa, R. 2013 Obtaining accurate mean velocity measurements in high reynolds number turbulent boundary layers using pitot probes. *Journal of Fluid Mechanics* **715** (1), 642–670.
- Chakraborty, N. & Swaminathan, N. 2013 Reynolds number effects on scalar dissipation rate transport and its modeling in turbulent premixed combustion. *Combustion Science and Technology* **185** (4), 676–709.
- DeGraaff, D. B., Webster, D. R. & Eaton, J. K. 1998 The effect of reynolds number on boundary layer turbulence. *Exp. thermal and fluid science* **18** (4), 341–346.
- del Álamo, J. C. & Jiménez, J. 2003 Spectra of the very large anisotropic scales in turbulent channels. *Phys. Fluids* **15** (6), 41–44.
- Den Toonder, J. M. J. & Nieuwstadt, F. T. M. 1997 Reynolds number effects in a turbulent pipe flow for low to moderate re. *Physics of Fluids* **9**, 3398.
- Ferchichi, M. & Tavoularis, S. 2000 Reynolds number effects on the fine structure of uniformly sheared turbulence. *Physics of Fluids* **12**, 2942.
- Hawkes, E. R., Sankaran, R., Sutherland, C. & H., Chen J. 2007 Scalar mixing in direct numerical simulations of temporally evolving plane jet flames with skeletal co/h<sub>2</sub> kinetics. *Proc. Combust. Inst.* **31**, 1633–1640.
- Hong, J., Katz, J. & Schultz, M. P. 2011 Near-wall turbulence statistics and flow structures over three-dimensional roughness in a turbulent channel flow. *Journal of Fluid Mechanics* **667** (1), 1–37.
- Hoyas, S. & Jiménez, J. 2008 Reynolds number effects on the reynolds-stress budgets in turbulent channels. *Physics of Fluids* **20**, 101511.
- Peters, N. 2000 *Turbulent Combustion*. Cambridge press.
- Pouransari, Z., Brethouwer, G. & Johansson, A. V. 2011 Direct numerical simulation of an isothermal reacting turbulent wall-jet. *Phys. Fluids* **23** (085104).
- Pouransari, Z. & Johansson, A. V. 2011 Numerical investigation of wall heat transfer in turbulent reacting wall-jets. In *Seventh Intern. Symp. on Turbulence and Shear Flow Phenomena, Ottawa, Canada* (ed. S. Tavoularis).
- Pouransari, Z., Vervisch, L. & Johansson, A.V. 2013 Heat release effects on mixing scales of non-premixed turbulent wall-jets: a DNS study. *Int. J. Heat and Fluid Flows* **40**, 65–80.
- Schumacher, Jörg 2008 Reynolds number effects on the turbulent mixing of passive scalars. In *IUTAM Symposium on Computational Physics and New Perspectives in Turbulence*, pp. 85–90. Springer.
- Vervisch, L. & Poinso, T. 1998 Direct numerical simulation of non-premixed turbulent flames. *Ann. Rev. Fluid Mech.* **30**, 655–691.
- Wei, T & Willmarth, WW 1989 Reynolds-number effects on the structure of a turbulent channel flow. *Journal of Fluid Mechanics* **204**, 57–95.
- Yiu, M. W., Zhou, Y., Zhou, T. & Cheng, L. 2004 Reynolds number effects on three-dimensional vorticity in a turbulent wake. *AIAA Journal* **42**(5), 1009–1016.